Anomalous magnetoresistance in the spinel superconductor $LiTi_2O_4$

K. Jin[1,2,3], G. He[1], X. Zhang[3,4], S. Maruyama[4], S. Yasui[4], R. Suchoski[4], J. Shin[4], Y. Jiang[3], H.S. Yu[1], J. Yuan[1], L. Shan[1,2], F.V. Kusmartsev[5], R. L. Greene[3], I.Takeuchi[4]

[1]Beijing National Laboratory for Condensed Matter Physics, Institute of Physics, Chinese Academy of Sciences, Beijing 100190, China

[2]Collaborative Innovation Center of Quantum Matter, Beijing, 100190, China

[3]Center for Nanophysics and Advanced Materials and Department of Physics, University of Maryland, College Park, Maryland 20742, USA

[4]Department of Materials Science and Engineering, University of Maryland, College Park, Maryland 20742, USA

[5]Department of Physics, Loughborough University, Loughborough LE11 3TU, United Kingdom

Transition-metal oxides offer great opportunity to explore unconventional superconductivity interrelated with novel phenomena such as spin/charge order, fluctuations, and Fermi surface instability. A systematic investigation of charge transport on the only known spinel oxide superconductor $LiTi_2O_4$ (LTO) has thus far prevented due to the lack of high quality single crystals. Here, we report a careful study of transport and tunneling spectroscopy in epitaxial LTO thin films. An unusual magnetoresistance (MR) is observed from nearly isotropic negative to prominently anisotropic positive as temperature decreases. The negative MR likely stems from the suppression of local spin fluctuations or spin-orbit scattering centers. The positive one is suggestive of the presence of an orbital related state, also supported by the fact that the superconducting energy gap decrease as a quadratic function of magnetic field. These observations indicate that spin/orbital fluctuations play an important role in LTO in a manner similar to high temperature superconductors.

$LiTi_2O_4$ (LTO) is the only known superconducting transition-metal oxide with a spinel crystal structure[1]. It was discovered in early 1970's by Johnston *et al* [2] with a superconducting transition temperature $T_c \sim 11$ K. Although its T_c can be described by band-structure calculations using the McMillan formula with a weak electron-phonon coupling constant ($\lambda_{el\text{-}ph}$~0.6) (refs 3,4), an enhanced density of states or an equivalently larger coupling constant has been unveiled from specific-heat[5,6] and magnetic susceptibility measurements[7]. Other measurements like nuclear magnetic resonance[8], point contact Andreev reflection spectroscopy[9], and resonant inelastic soft-

x-ray scattering[10] have revealed the significance of *d*-*d* electron correlations. It is naturally expected whether such correlations play an important role in the microscopic mechanism for its superconductivity.

Moreover, in contrast to oxide perovskites, LTO has a cubic symmetry with the space group of *Fd3m*, in which the lithium and titanium cations are located at the tetrahedral 8a and octahedral 16d sites, respectively. On one hand, the t_{2g} sub-band of Ti is in high degree of degeneracy, remaining in a narrow d-band metal with significant electron-electron interaction[8,11]. On the other hand, the Ti sublattice, in mixed valences of Ti^{3+} and Ti^{4+}, is frustrated and favors short-range spin ordering[12]. Therefore, LTO is highly complementary to the perovskite-type high temperature superconductor, where the unconventional superconductivity is intimately related to spin/orbital fluctuations[13,14]. However, the development of an understanding of this system has being hampered by the lack of sample reproducibility and the availability of single crystals or high quality thin films[1,7,15]. Recently, high quality epitaxial LTO thin films successfully grown by pulsed laser deposition (PLD) have been demonstrated[16,17], thus opening the door for systematic experiments on LTO.

In this paper, we present results of transport and tunneling studies on single crystalline-like epitaxial LTO thin films. The suppression of the superconducting energy gap as a quadratic function of magnetic field, and an anomalous crossover of magnetoresistance from prominently anisotropic positive to nearly isotropic negative with increasing temperature have been observed for the first time. In addition to the extracted key parameters from the combined tunneling and transport measurements, a full picture of LTO has emerged: the data suggest the presence of spin-orbit scattering/spin fluctuations below ~ 100±10 K and an orbital related state below T_{ch} ~ 50±10 K, based on which a theoretical model is proposed to account for the relation between the superconducting energy gap and the magnetic field.

Results

Charge transport data and tunneling spectra. The (00*l*)-Oriented LTO thin films were epitaxially grown on (00*l*)-oriented $MgAl_2O_4$ (MAO) substrates by PLD. Our LTO films consistently display T_c of 11 ± 0.25 K with narrow transition widths of less than 0.5 K. We have found that different films have different residual resistivity ratios (*RRR*). The films were

patterned into Hall-bars to carry out Hall and normal resistivity measurements. Tunneling spectroscopy was performed where Pt-Ir tips were used to make point contacts in the out-of-plane axis direction (*c*-axis, perpendicular to the film plane) of LTO[18].

Fig. 1(a) shows the resistivity versus temperature curves for samples with two different *RRR* ratios: 6.25 and 3 for samples L1 and L2, respectively. L1 and L2 have similar resistivity values at the room temperature and the same T_c. The normal state resistivity of both samples can be fitted to a curve consistent with the Fermi liquid behavior, $\rho = \rho_0 + AT^2$ (gray lines) from 40 K to 120 K with residual resistivity (ρ_0) of $\approx 71\ \mu\Omega$ cm for L1 and $\approx 166\ \mu\Omega$ cm for L2. The deviation from the Fermi liquid behavior at low temperatures is caused by an enhanced electron-electron interaction as discussed below. By sweeping the magnetic field perpendicular to the film surface [$B \perp$ in-plane (*ab* plane)] at fixed temperatures, the Hall resistivity, i.e. $\rho_{xy} = \frac{E_y}{j_x} = \frac{V_y.t}{I_x}$, has been extracted. ρ_{xy} data for different temperatures are plotted in Fig. 1(b), where V_y is the Hall voltage obtained by subtracting the transverse voltage in negative field from that in positive field, and t is the thickness of the film. In the normal state, the Hall resistivity is always proportional to the magnetic field, positive and temperature independent, strongly suggesting the presence of one type of charge carriers (holes) and a simple electronic band structure. The charge carrier concentration is calculated assuming a parabolic band structure, i.e., the Hall coefficient $R_H = \frac{1}{ne}$. L1 and L2 have almost the same hole concentration of $\sim 3\times10^{22}$ cm^{-3} [Fig. 1(c)], indicating that the different *RRRs* are likely caused by the difference in mobility values.

The point contact measurements were carried out on L1 before it was patterned into a Hall bar for transport measurements. As described by Blonder, Tinkham, and Klapwijk (BTK) (ref. 19), the tunneling regime is achieved for Z > 1, where Z represents the tunneling barrier height and the Fermi velocity mismatch[20]. The differential conductance spectrum shows a clear temperature and field dependent coherence peak. The normalized differential conductance spectra with and without applied magnetic field are shown in Fig. 2(a), (b), and (c) as a function of bias voltage (see ***SI*** for raw data and normalization procedure). The normalized experimental curves were fitted using a modified BTK model with a complex energy $E' = E + i\Gamma$ (ref. 21). The broadening Γ term, which takes into account sample inhomogeneity and a finite quasi-particle lifetime by

scattering, is temperature independent in zero field, but application of magnetic field has been found to lead to an additional pair breaking factor[22], which in effect is akin to an enhanced Γ (ref. 23).

Fitting parameters and superconducting energy gap. Several key points could be made from the fitting of our tunneling spectra. *Firstly*, the Z value of our Pt-Ir/LTO junction is ~ 2.4, which is independent of temperature and field. *Secondly*, zero-field spectra give a constant Γ of ~ 0.94 meV (Supplementary Fig. 2), but data in field have to be fitted with an increasing Γ as the field is increased (Supplementary Fig. 3). *Thirdly*, the temperature dependence of the superconducting energy gap can be fitted well with the BCS theory (Fig. 2(d)), and the observed $2\Delta_0/k_BT_c = 4$ (Δ_0 = 1.93 meV) is consistent with previous reports[6,9], indicating that LTO is a medium-coupling BCS superconductor. Moreover, a simple relation of $\Delta(B, T)/\Delta(0\ \mathrm{T}, T) \sim -[B/B_{c2}(T)]^2$, can be used to scale the field dependent energy gap at different temperatures, e.g. T = 2, 6, 10 K (Fig. 2(e)). Accordingly, B_{c2} can be extracted from the point contact spectra, and it is $B_{c2}(2\mathrm{K}) \sim 16$ T.

We also employed a two-channel method derived from the BTK model to fit our experimental data[24]. In this method, the pair-breaking effect by field is considered as a normal channel (N) superposed onto the superconducting channel (S). Assuming the differential conductance to take the form $G(h) = h^r G_N + (1 - h^r)G_S$ with $h = B/B_{c2}$, the normalized differential conductance in field should obey the polynomial form $\frac{G(h)}{G_N} = h^r + (1 - h^r)\frac{G_S}{G_N}$, where $\frac{G_S}{G_N}$ is obtained from the BTK model with a constant Γ. The best fitting requires $r = 2$. We note that this value is consistent with those used to fit data for point contacts with other superconductors such as Nb, Mo_3Sb_7, and $Dy_{0.8}Y_{0.2}Rh_4B_4$ (ref. 24). In this case, the relation, $\Delta(B) \sim -B^2$ emerges again, and the Δ values extracted from the two fitting methods are similar (Figure 2(e)).

To the best of our knowledge, none of the existing theoretical models can account for the quadratic relation. When B is close to B_{c2}, the Maki formula[25] can be analytically expressed as $\overline{|\Delta|}^2 \sim \frac{B_{c2}-B}{\Psi_2(\frac{1}{2}+\frac{A}{2\pi k_B T})}$, where $\bar{\Delta}$ represents the averaged energy gap taking into account the effect of vortices, and Ψ_2 is the first derivative of the digamma function with A the pair breaking parameter proportional to B when $B \perp ab$ plane[26]. But, this does not lead to a quadratic field dependence of the superconducting energy gap.

Theoretical model. We note, however, that if there exists an additional anisotropy axis, which breaks the intrinsic symmetry of the system, e.g. orbital ordering or a background nematicity, $\Delta(B) \sim -B^2$ can arise. To simplify the discussion without loss of generality, we assume that the superconducting order parameter is a 3-component vector, $\mathbf{\Delta} = (\Delta_x, \Delta_y, \Delta_z)$. Then the isotropic gap is equal to the modulus of this vector: $\Delta_0 = \mathbf{(\Delta \cdot \Delta)^{1/2}} = (\Delta_x^2 + \Delta_y^2 + \Delta_z^2)^{1/2}$. In zero field, the orientation of the local spin of the Cooper pair changes in real space, while the value of the gap does not change. Therefore, the average magnetic moment of Cooper pairs vanishes, that is $\langle \mathbf{\Delta(r)} \rangle = \mathbf{0}$. However, in magnetic field, $\boldsymbol{B}$, the magnetic moments of Cooper pairs can be partially polarized and therefore the susceptibility, χ, can develop a paramagnetic component, so that $\chi_{super} = \chi_{para} + \chi_{dia}$. Here, the last term is the conventional diamagnetic susceptibility of a superconductor.

The first term χ_{para} should be a function of the magnetic moments of the Cooper pairs which contribute to the symmetry invariants. There are in general three symmetry invariants here. The first one is just $\mathbf{\Delta \cdot \Delta}$, the second one is $\mathbf{\Delta \cdot} \boldsymbol{B}$. The additional anisotropy axis, e.g. orbital ordering or background nematicity associated with some vector **b** results in another invariant as $\mathbf{\Delta \cdot b}$. In the vicinity of the phase transition, we can use the Taylor expansion to obtain:

$$\chi_{para}((\mathbf{\Delta \cdot b}), (\mathbf{\Delta \cdot} \boldsymbol{B})) = \chi_{para}(0, 0) + \chi'_{para}(0, 0)\,(\mathbf{\Delta \cdot b}) + \chi'_{para}(0, 0)\,(\mathbf{\Delta \cdot} \boldsymbol{B}) + (\text{high order terms}) \quad (1)$$

In using this expression, the total free energy of the superconductor in the lowest order with superconducting order parameter can be written in the form:

$$F(\mathbf{\Delta}) = \alpha\,(\mathbf{\Delta \cdot \Delta}) + 2\delta\,(\mathbf{\Delta \cdot b})\,(\boldsymbol{B \cdot B}) + \mu\,(\boldsymbol{B \cdot B}) + (\text{ high order terms}) \quad (2)$$

Minimization of the free energy with respect to $\mathbf{\Delta}$ will give the expression $\Delta(B) = \mathbf{(\Delta \cdot \Delta)^{1/2}} = (-\alpha/2\beta)^{1/2} - \delta\, b\, B^2/2|\alpha|$ where α, β, δ are the parameters of the Ginzburg-Landau expansion, and b is the modulus of the vector **b** (See ***SI*** for details). This represents the first plausible explanation giving rise to the relation, $\Delta(B) \sim -B^2$. As for the origin of the symmetry breaking which gives rise to the vector **b** in LTO, we propose that there is an onset of orbital ordering which takes place in LTO below a transition temperature T_{ch}, arising from orbital degeneracy of t_{2g} sub-band[27,28].

We would like to point out that although this relation has not been carefully examined previously, we also observe it in some cuprates, namely, electron-doped $(Nd, Ce)_2CuO_4$ and $(Pr, La, Ce)_2CuO_4$ (Supplementary Fig. 4, see ***SI*** for details), indicating the presence of a similar

symmetry breaking ordering in these compounds. We believe other ordering mechanisms such as spin stripes or charge density wave may also lead to a symmetry breaking resulting in the vector **b**. However, the relation from the Maki formula was obeyed in superconductors without symmetry breaking, e.g. $\Delta^2(B) \sim -B$ or $-B^2$ for Zn (ref. 29) and $\Delta^2(B) \sim -B$ $(Ba,K)BiO_3$ (ref. 30). The electronic nematicity has been widely discussed in hole-doped cuprates[31,32] and Fe-based superconductors[33,34], which acts as a competing order to the superconductivity. The exact nature of the ordering in electron-doped cuprates is beyond the scope of the present work[35], but the discovered quadratic relation is perhaps rather common in different types of superconductors. It would therefore be of broad interest to investigate the occurrence of this relation in other superconductors also: it can possibly serve as a signature underpinning different mechanisms leading to intrinsic symmetry breaking, which results in the presence of an additional anisotropy axis.

Zero bias conductance. The normalized zero bias conductance (ZBC) at 2 K and 6 K shows a linear dependence on the magnetic field (see ***SI*** for calculation details), indicating a linear increase of the vortex density with uncorrelated vortices (Fig. 2(f)). Such a relation has been reported in systems such as $Bi_2Sr_2CaCu_2O_{8+\delta}$ overdoped with intercalating $HgBr_2$ molecules[36] and in nanosized Pb islands on a silicon wafer[37]. The departure from linearity in field-dependent ZBC has previously been observed in MgB_2 (ref. 38) and YNi_2B_2C (ref. 39), associated with the fact that they are multiband superconductors. In the $Ca_{2-x}Na_xCuO_2Cl_2$ (x = 0.14), the field dependence scales as $B\log B$, suggested to be an indication of a dirty d-wave superconductor[40]. Previous specific heat experiments have suggested that LTO is an s-wave superconductor[6]. Thus, based on the lack of departure from the linearly dependent ZBC, we conclude that LTO is not likely to be a multiband superconductor.

Calculated key physical quantities. Combining the transport and tunneling data, we were able to extract key parameters for LTO. The Ginzburg-Landau coherence length, the size of the vortex core in type II superconductor is estimated to be $\xi_{GL} = (\frac{\Phi_0}{2\pi B_{c2}})^{1/2} = 4.47\ nm$. The mean free path of $l = 1.8\ nm$ is deduced from the Drude model $\rho_0 = \frac{\hbar k_F}{ne^2 l}$, where the Fermi wave-vector $k_F = (3\pi^2 n)^{1/3} = 0.96\ \text{Å}^{-1}$. Since $l < \xi_{GL}$, the BCS coherence length of $\xi_{BCS} = 14.9\ nm$ is

calculated from the dirty limit relation, $\xi_{GL} = \frac{0.855\times(\xi_{BCS}l)^{1/2}}{(1-\frac{T}{T_c})^{1/2}}$. We then calculate the Fermi velocity from the formula, $\xi_{BCS} = \hbar v_F/\pi\Delta$, and arrive at an effective mass of m^*/m_0 = 8.11 (with m_0 being the free electron mass), and the density of states at the Fermi level is found to be $N(E_F)$ = 0.96 states/eV atom.

We compared these parameters to those obtained from previous reports on LTO. Only T_c and ξ_{GL} values have been previously reported on thin films[16], and the other quantities were from the magnetic susceptibility[7], Andreev reflection[9], and specific heat[6] measurements on polycrystalline samples. As seen in Table 1, the values obtained in the present work are consistent with those from previous reports. We note that in polycrystalline samples, the grain boundaries prevent accurate calculations from the transport measurements due to boundary scattering, but the parameters could be extracted from heat capacity and susceptibility data. These values indicate that the nearly free electron model can capture the main physics of the LTO system.

Field-direction dependence of magnetoresistivity. In the normal state, however, we observe an anomalous MR behavior. Figure 3(a) illustrates the field dependent MR in sample L1 when $B \perp ab$ plane. The MR gradually decreases from positive to negative with increasing temperature, and a crossover is observed at 50±10 K. In the inset of Figure 3(a), the MR is plotted as B^2. The positive MR is proportional to B^2 whereas the negative MR is not. In the case of $B \perp ab$ plane, both orbital and spin effects can contribute to MR, and in order to discern the different contributions, additional measurements were carried out where the field was also applied in the film plane with $B \,//\, I$ (parallel to current) and $B \perp I$ (normal to current). In Fig. 3(b), the temperature dependence of MR is plotted for both L1 (gray symbols) and L2 (red symbols). The negative MR is nearly independent of the field directions, but the positive MR displays unambiguous anisotropy, i.e. MR ($B \perp$ ab plane) > MR (B // ab-plane, $B \perp I$) > MR (B // ab-plane // I). Moreover, the MR changes its sign when $B \,//\, I$, as seen in Figure 4(a). The first derivative of ρ_{xx}(T) in zero field (symbols) starts to deviate from the Fermi liquid behavior ($d\rho_{xx}/dT \sim T$) at roughly the same range of temperature as seen in Fig. 4(b), indicating the presence of an enhanced electron-electron interaction.

Such transport data collectively point to the presence of a phase transition with a characteristic temperature T_{ch} of ~ 50±10 K. As discussed above, we believe orbital ordering results in the

relation, $\Delta(B) \sim -B^2$. Thus, we associate T_{ch} with the onset of an orbital related state such as orbital ordering or nematicity (see ***SI***). If the LTO system indeed has such a symmetry breaking feature, it should also manifest itself in the anisotropy of the in-plane angular dependent magnetoresistivity (AMR) measurements, and a two-fold symmetry would be expected, similar to the case of iron arsenide superconductors[41]. We indeed observe a two-fold AMR in LTO (Fig. 4(e)). Note that a strong enhancement in amplitude of the two-fold symmetry takes place below T_{ch}: we associate this with the orbital related ordering. On the other hand, we find that the starting temperature of the two-fold AMR is around 100±10 K, far above the T_{ch}.

Temperature dependence of magnetic susceptibility. To understand this discrepancy, we also measured the temperature dependent susceptibility in zero-field and field cooling. The $\chi(T)$ in zero-field cooling data shows a clear screening effect due to superconductivity below 11 K (Fig. 4(e)). In field cooling, we find that the residual susceptibility, $\delta\chi(T)$, found by subtracting a paramagnetic component from the $\chi(T)$, starts to increase below 100±10 K (Fig. 4(d)), corresponding to the same temperature where the two-fold symmetry emerges. The amplitude of the two-fold symmetry exhibits an abrupt increase at T_{ch} = 50±10 K. We, thus, attribute the two-fold AMR to two sources: one related to a spin interaction starting at a higher temperature (100±10 K), and the other associated with an orbital effect (discussed below) becoming pronounced below T_{ch} = 50±10 K.

Our findings, thus far, can be summarized in the following three points: 1) With decreasing temperature, the magnetic susceptibility increases and deviates from the Curie-Weiss behavior below 100±10 K, while the in-plane AMR starts to show a two-fold symmetry and the magnetoresistivity is negative in field; 2) At $T_{ch} \sim$ 50±10 K, the sign of magnetoresistivity changes to positive and the two-fold symmetry becomes more prominent, where we also observe deviation from the Fermi liquid behavior; 3) Below 11 K, LTO enters the superconducting state, where the superconducting energy gap decreases as a function of B^2.

Discussion

Generally, MR can result from charge, orbital, or spin interactions, as well as interactions among them[42]. First of all, the observed constant Hall coefficient and smooth temperature evolution of the *c*-axis lattice parameter (Supplementary Fig. 8) preclude the presence of charge density

waves, which normally influences the Hall coefficient[43]. The mean free path of the "clean" sample (L1) is 1.84 nm in the zero-temperature limit, which is only about two unit cells of the LTO lattice. Therefore, a grain boundary effect is unlikely to have a dominant role in the MR behavior. The combination of Points 2) and 3) above supports an orbital effect as the origin of the positive anisotropic MR below 50±10 K, which introduces the additional anisotropic axis in the system used in the theoretical model. The temperature at which the two-fold AMR at 100±10 K emerges corresponds to the temperature where the increase in antiferromagnetic-like spin correlation takes place (and where the Curie-Weiss fitting intercepts the temperature axis at negative value), indicating that the negative MR is associated with a spin interaction. We note that in $La_{2-x}Ce_xCuO_4$ thin films, AFM has been identified as the main cause of a two-fold symmetry of AMR and a negative MR (ref. 44), while in Fe-based superconductors, the anisotropy of in-plane charge transport is found to be associated with the nematic order[41]. Although the spinel structure is quite different from the perovskite one, the appearance (100±10 K) and the sudden enhancement (50±10 K) of two fold symmetry of AMR in LTO link local AFM correlations and orbital related state, respectively.

In antiferromagnetic metals, a sign change in MR is expected theoretically at the Neel temperature due to the *s-d* electron interaction[45]. However, this idea is based on long range antiferromagnetism (AFM), and the change in sign from negative to positive is to be accompanied by a discontinuous jump in MR. This is in contrast to the observation in LTO, where there is no discontinuous jump. Moreover, the LTO system has a frustrated Ti sublattice containing equal numbers of Ti^{3+} and Ti^{4+}, and thus a long range AFM ordering is unfavorable[12]. The emergence of short-range AFM ordering has been reported in V-doped LTO by nuclear magnetic resonance[11] and in LiV_2O_4 by inelastic neutron scattering[46]. Note that the AMR measurements cannot be used to tell whether the AFM is static or dynamic. It is possible that local spin fluctuations are responsible for the negative MR.

We consider an alternative explanation due to the effect of spin-orbit coupling. When the orbital ordered (nematic) state is destroyed at $T > T_{ch}$, some "fluctuating" islands may have a finite life time and serve as additional (magnetic) scattering centers for the electron transport. When the magnetic field is applied, some of these islands disappear and the resistivity decreases. This is exemplified in thin metallic Mg films covered with small controlled quantities of a magnetic ion

such as Fe, or a heavy ion with large spin-orbit coupling such as Au: the magnetoresistance changes its sign from negative to positive upon experiencing an increase in the number of spin-orbit scattering centers[47]. Perhaps a similar mechanism is at work in LTO.

In conclusion, detailed properties of superconducting LTO were investigated for the first time in high quality thin films. Many properties are consistent with previous work on polycrystalline samples: we observe one type of charge carrier and a $\frac{2\Delta}{k_B T_c}$ value consistent with a medium-coupling BCS superconductor. The main physics can be captured by the nearly free electron model. However, we find two new and distinct features in this system. In the superconducting state, a scaling law, $\Delta(B) \sim -B^2$ at $T < T_c$, is extracted from our point contact spectra. This behavior had not been predicted by any previous theory. In the normal state, an anomalous MR which crosses over from nearly isotropic negative MR to an anisotropic positive MR with decreasing temperature is observed. The anisotropic positive MR likely originates from the enhanced electron-electron interaction due to the orbital related ordering below $T_{ch} \sim 50\pm10$ K. The negative MR occurring at 100±10 K possibly stems from the suppression of spin-orbit scattering or local spin fluctuations. We present a new theoretical model based on the proposal that there is orbital ordering in the superconducting state to account for the relation $\Delta(B) \sim -B^2$. The fact that this relation is also observed in other materials ($(Nd, Ce)_2CuO_4$ and $(Pr, La, Ce)_2CuO_4$) points to the broader applicability of the model developed here in understanding underlying interactions in different types of superconductors.

Acknowledgements

We would like to thank Y. Dagan, Y. Nakajima, J. Paglione, P. Dai, G. Zheng, and K. Liu, Z. Meng for useful discussions. This research was supported by the National Science Foundation (1104256), AFOSR-MURI (FA9550-09-1-0603), AFOSR (FA95501410332), the Strategic Priority Research Program (B) of the Chinese Academy of Sciences (XDB07020100), and National Natural Science Foundation of China Grant (11474338, 11322432).

Author contributions

K.J., R.L.G., and I.T. designed research; S.M., S.Y., R.S., and J.S. prepared the thin films; K.J. performed transport and point contact measurements; X.Z., Y.J., H.S.Y., and J.Y. complemented

transport measurements; K.J., G.H., L.S., F.V.K., and R.L.G. analyzed data; K. J., R.L.G., and I.T. wrote the paper.

Additional information

Competing financial interests: The authors declare no competing financial interests.

E-mails: kuijin@iphy.ac.cn, rgreene@squid.umd.edu, takeuchi@umd.edu.

References

1. Moshopoulou, E. G. Superconductivity in the spinel compound $LiTi_2O_4$. *J. Am. Ceram. Soc.* **82**, 3317-3320 (1999).

2. Johnston, D. C., Prakash, H., Zacharia.Wh & Viswanat. R. High-temperature superconductivity in Li-Ti-O Ternary system. *Mater. Res. Bull.* **8**, 777-784 (1973).

3. Massidda, S., Yu, J. J. & Freeman, A. J. Electronic-structure and properties of superconducting $LiTi_2O_4$. Phys. Rev. B **38**, 11352-11357 (1988).

4. Satpathy, S. & Martin, R. Electronic structure of the superconducting oxide spinel $LiTi_2O_4$. *Phys. Rev. B* **36**, 7269-7272 (1987).

5. Johnston, D. C., Swenson, C. A. & Kondo, S. Specific heat (1.2–108 K) and thermal expansion (4.4–297 K) measurements of the 3d heavy-fermion compound LiV_2O_4. *Phys. Rev. B* **59**, 2627-2641 (1999).

6. Sun, C. P. *et al*. Magnetic field dependence of low-temperature specific heat of the spinel oxide superconductor $LiTi_2O_4$. *Phys. Rev. B* **70**, 054519 (2004).

7. Johnston, D. C. Superconducting and normal state properties of spinel compounds, I. Preparation, crystallography, superconducting properties, electrical resistivity, dielectric behavior, and magnetic susceptibility, *J. Low Temp. Phys.* **25**, 145-175 (1976).

8. Tunstall, D. P. *et al*. Titanium nuclear magnetic resonance in metallic superconducting lithium titanate and its lithium-substituted derivatives $Li_{1+x}Ti_{2-x}O_4$ ($0 < x < 0.10$). *Phys. Rev. B* **50**, 16541-16549 (1994).

9. Tang, L. *et al*. Electrical resistivity and Andreev reflection spectroscopy of the superconducting oxide spinel $LiTi_2O_4$. *Phys. Rev. B* **73**, 184521 (2006).

10. Chen, C. L. *et al*. Role of 3d electrons in the rapid suppression of superconductivity in the dilute V doped spinel superconductor $LiTi_2O_4$. *Supercond. Sci. & Tech.* **24**, 115007 (2011).

11. Itoh, Y., Moritsu, N. & Yoshimura, K. Emergence of Antiferromagnetic Correlation in $LiTi_{2-x}V_xO_4$ via ^{7}Li NMR. *J. Phys. Soc. Jpn.* **77**, 123713 (2008).

12. Anderson, P. W. Ordering and antiferromagnetism in ferrites. *Phys. Rev.* **102**, 1008-1013 (1956).

13. Jin, K., Butch, N. P., Kirshenbaum, K., Paglione, J. & Greene, R. L. Link between spin fluctuations and electron pairing in copper oxide superconductors. *Nature* **476**, 73-75 (2011).

14. Paglione, J. & Greene, R. L. High-temperature superconductivity in iron-based materials. *Nature Phys.* **6**, 645-658 (2010).

15. Inukai, T., Murakami, T. & Inamura, T. Preparation of superconducting $LiTi_2O_4$ thin films. *Thin Solid Films* **94**, 47–50 (1982).

16. Chopdekar, R. V. *et al*. Growth and characterization of superconducting spinel oxide $LiTi_2O_4$ thin films. *Physica C* **469**, 1885-1891 (2009).

17. Kumatani, A. *et al*. Growth processes of lithium titanate thin films deposited by using pulsed laser deposition. *Appl. Phys. Lett.* **101**, 123103 (2012).

18. Diamant, I., Hacohen-Gourgy, S. & Dagan, Y. Evolution of a bosonic mode across the superconducting dome in the high-T_c cuprate $Pr_{2-x}Ce_xCuO_{4-\delta}$. *Phys. Rev. B* **84**, 104511 (2011).

19. Blonder, G. E., Tinkham, M. & Klapwijk, T. Transition from metallic to tunneling regimes in superconducting microconstrictions: Excess current, charge imbalance, and supercurrent conversion. *Phys. Rev. B* **25**, 4515-4532 (1982).

20. Blonder, G. E. & Tinkham, M. Metallic to tunneling transition in Cu-Nb point contacts. *Phys. Rev. B* **27**, 112-118 (1983).

21. Dynes, R., Garno, J., Hertel, G. & Orlando, T. Tunneling study of superconductivity near the metal-Iinsulator transition. *Phys. Rev. Lett.* **53**, 2437-2440 (1984).

22. Bandte, C., Hertel, P. & Appel, J. Pair-breaking effects in high-temperature superconductors. *Phys. Rev. B* **45**, 8026-8035 (1992).

23. Daghero, D. & Gonnelli, R. S. Probing multiband superconductivity by point-contact spectroscopy. *Supercond. Sci. & Tech.* **23**, 043001 (2010).

24. Smith, C. W. & Dolan, P. J. Determining transport parameters for superconductor/normal metal point contacts at fixed temperature from conductance versus magnetic field data. *Physica C* **471**, 285-289 (2011).

25. Maki, K. Physics. Long Island City, New York, **1**, 21 (1964).

26. Tinkham, M. Introduction to superconductivity (second edition), chapter 10. Mineola, New York (2004).

27. Laad, M. S., Bradarić, I. & Kusmartsev, F. V. Orbital non-Fermi-liquid behavior in cubic ruthenates, *Phys. Rev. Lett.* **100**, 096402 (2008).

28. Kusmartsev, F.V. Formation of electron strings in narrow band polar semiconductors. *Phys. Rev. Lett.* **84**, 530-533 (2000).

29. Naidyuk, Y. G., Löhneysen, H. v. & Yanson, I. K. Temperature and magnetic-field dependence of the superconducting order parameter in Zn studied by point-contact spectroscopy. *Phys. Rev. B* **54**, 16077-16081 (1996).

30. Szabó, P. *et al*. Magnetic pair breaking in superconducting $Ba_{1-x}K_xBiO_3$ investigated by magnetotunneling. *Phys. Rev. B* **62**, 3502-3507 (2000).

31. Daou, R. *et al*. Broken rotational symmetry in the pseudogap phase of a high-T_c superconductor. *Nature* **463**, 519-522 (2010).

32. Vojta, M. Lattice-symmetry breaking in cuprate superconductors: stripes, nematics and superconductivity. *Adv. Phys.* **58**, 699-820 (2009).

33. Baek, S. -H. *et al*. Orbital-driven nematicity in FeSe. *Nature Mater.* **14**, 210-214 (2015).

34. Kontani, H. & Yamakawa, Y. Linear response theory for shear modulus C_{66} and Raman quadrupole susceptibility: evidence for nametic orbital fluctuations in Fe-based superconductors. *Phys. Rev. Lett.* **113**, 047001(2014).

35. Armitage, N. P., Fournier, P. & Greene, R. L. Progress and perspectives on the electron-doped cuprates. *Rev. Mod. Phys.* **82**, 2421-2487 (2010).

36. Krasnov, V. M., Kovalev, A. E., Yurgens, A. & Winkler, D. Magnetic field dependence of the superconducting gap and the pseudogap in Bi2212 and HgBr2-Bi2212, studied by intrinsic tunneling spectroscopy. *Phys. Rev. Lett.* **86**, 2657-2660 (2001).

37. Ning, Y. X. *et al*. Observation of surface superconductivity and direct vortex imaging of a Pb thin island with a scanning tunneling microscope. *Europhys. Lett.* **85**, 27004 (2009).

38. Eskildsen, M. R. *et al*. Scanning tunneling spectroscopy on single crystal MgB_2. *Physica C* **385**, 169 (2003).

39. Mukhopadhyay, S., Sheet, G., Raychaudhuri, P., & Takeya, H. Magnetic-field dependence of superconducting energy gaps in YNi_2B_2C: Evidence of multiband superconductivity. *Phys. Rev. B* **72**, 014545 (2005).

40. Hanaguri, T. *et al*. Coherence factors in a high-T_c cuprate probed by quasi-particle scattering off vortices. *Science* **323**, 923-926 (2009).

41. Chu, J. H. *et al*. In-plane resistivity anisotropy in an underdoped iron arsenide superconductor. *Science* **329**, 824-826 (2010).

42. Imada, M., Fujimori, A. & Tokura, Y. Metal-insulator transitions. *Rev. Mod. Phys*. **70**, 1039–1263 (1998).

43. Daou, R. *et al*. Linear temperature dependence of resistivity and change in the Fermi surface at the pseudogap critical point of a high-T_c superconductor. *Nature Phys.* **5**, 31–34 (2009).

44. Jin, K. *et al*. Evidence for antiferromagnetic order in $La_{2-x}Ce_xCuO_4$ from angular magnetoresistance measurements. *Phys. Rev. B* **80**, 012501 (2009).

45. Yamada, H. & Takada, S. Magnetoresistance of antiferromagnetic metals due to s-d interaction. *J. Phys. Soc. Jpn.* **34**, 1 (1973).

46. Lee, S. H., Qiu, Y., Broholm, C., Ueda, Y. & Rush, J. Spin fluctuations in a magnetically frustrated metal LiV_2O_4. *Phys. Rev. Lett.* **86**, 5554-5557(2001).

47. Bergman, G. Measurement of the magnetic scattering time by weak localization. *Phys. Rev. Lett.* **49**, 162-164 (1982).

Table 1. Physical parameters of $LiTi_2O_4$ obtained in present work and comparison to values from previous work.

	T_c (K)	Δ(meV)	ξ_{BCS}(nm)	ξ_{GL}(nm)	n (cm^{-3})	m^*/m_0	l(nm)	v_F(m/s)	N(E_F)
Present	11±0.25	1.93±0.01	14.9	4.47	3×10^{22}	8.11	1.84	1.37×10^{5}	0.96
Previous	11.5±0.5	1.9	-	4.1-4.6	1.35×10^{22}	9.4	3.2	-	0.97

The quantities in the present work were obtained from transport and tunneling results on Sample L1. Since most of the earlier studies were carried out on polycrystalline samples, the parameters such as carrier density (n), effective mass (m^*), and density of states (N(E_F): states/eV.atom) are from previous magnetic susceptibility measurements using nearly free electron approximations[7]. The mean free path (l) was calculated from the specific heat data[6]. We compare the Ginzburg-Landau coherence length (ξ_{GL}) to the value reported by another thin film study[16], and the superconducting energy gap (Δ) to the value obtained from an Andreev study on polycrystalline samples[9].

Figure 1 Resistivity, Hall resistivity and Hall coefficient of $LiTi_2O_4$ thin films. (a) plots $\rho_{xx}(T)$ of two samples. They have similar resistivity (~500 μΩ cm) at room temperature, and the same T_c of 11 K, but different residual resistivity ratios (*RRR*): *RRR*~6.25 for Sample L1 (black curve) and ~ 3 for the Sample L2 (red curve). The resistivity curve from 40 to 120 K can be fit by $\rho = \rho_0 + AT^2$(gray lines). **(b)** The Hall resistivity is proportional to the magnetic field at different temperatures, and all the ρ_{xy}(B) curves overlap in the normal state (only data on Sample L1 are shown here), suggesting a simple one band structure and a temperature independent Hall coefficient. Note that at very low temperatures, the magnetic field is not sufficient to suppress the superconductivity ($B \perp$ ab plane). **(c)** Hall coefficient versus temperature for both samples (L1: solid symbols. L2: open symbols). Though the two samples show different *RRR*, their Hall coefficient values are very close to each other. Assuming $R_H = 1/(ne)$, we find a hole concentration of ~3×10^{22} cm^{-3} which is almost constant over the entire measured temperature range.

Figure 2 Temperature and field dependent tunneling spectroscopy curves and the superconducting energy gap of LTO films. (a) Normalized differential conductance versus bias voltage from 2 to 10.5 K (ΔT = 0.5 K) in zero field. Experimental data are fitted with a modified BTK model with a constant broadening Γ term (red lines), and are vertically shifted above the 2 K curve for clarity. **(b)** and **(c)** Normalized differential conductance versus field from 0 to 9 T at 2 K, and from 0 to 7 T at 6 K, respectively (ΔB = 1 T, $B \perp ab$ plane). Experimental data (gray circles) are fitted with a modified BTK model with an increasing Γ as *B* is increased (red lines), and also with the two-channel model (cyan lines). Data in fields are vertically shifted. **(d)** Temperature dependent energy gap values, $\Delta(T)$, are obtained from the BTK fits: $2\Delta/k_BT_c$ = 4 is obtained, indicating a medium-coupling BCS-like superconductor. **(e)** Normalized energy gap $[\Delta(B)/\Delta(0T)]$ decreases as $(B/B_{c2})^2$ in the superconducting state, and can be scaled for different temperatures. In-field measurements were carried out at *T* = 2, 6 and 10 K (open symbols extracted from modified BTK fittings with an increasing Γ and cross symbols from the two-channel model). **(f)** The normalized zero bias conductance (symbols) at 2 K and 6 K shows a linear dependence on the magnetic field (red straight fitting line). The error bars in (d), (e), and (f) represent the standard error in the fit to the data.

Figure 3 Temperature dependence of magnetoresistivity, $\Delta\boldsymbol{\rho_{xx}} = \boldsymbol{\rho_{xx}(B)} - \boldsymbol{\rho_{xx}(0T)}$. (a) The transverse magnetoresistivity with $B \perp$ ab plane, changes from negative to positive as temperature is decreased. The crossover temperature is ~ 50±10 K. The positive magnetoresistivity is proportional to B^2 as seen in the inset, whereas the

negative MR is not. **(b)** Magnetoresistivity at 7 T plotted against the temperature. The dark and red symbols are for samples L1 and L2, respectively. The magnetic field was applied along three different directions, i.e., *B* // *ab*-plane (*B* // I, *B* ⊥I) and *B* ⊥ *ab* plane. The negative magnetoresistivity is nearly isotropic, whereas the positive magnetoresistivity shows unambiguous anisotropy.

Figure 4 Magnetoresistivity, resistivity deviation, angular dependent in-plane resistivity, and susceptibility of $LiTi_2O_4$ thin films. (a) Temperature dependent longitudinal magnetoresistivity (*B* // *ab*-plane // I), $\Delta\rho_{xx} = \rho_{xx}(B) - \rho_{xx}(0\mathrm{T})$, is replotted to demonstrate the crossover temperature [also see Figure 3 (b)]. **(b)** $d\rho_{xx}/dT$ in zero field. It deviates from the Fermi liquid behavior, $d\rho_{xx}/dT \sim T$ (gray line), at lower temperatures. **(c)** The in-plane (*ab*-plane) resistivity starts to show two-fold symmetry below ~ 100 K, and become prominent at ~ 50±10 K with decreasing temperature. The inset shows a typical two fold symmetry at 30 K and 9 T against θ, which is the angle between the normal direction to current and the field. ρ_{max}： θ = 90°ρ_{min}： θ = 0°.**(d)** The susceptibility at field cooling (1000 Oe, *B* // *ab*-planein-plane) shows a Curie-Weiss behavior at high temperature [see inset $\chi^{-1}(T)$]. We plot the residual susceptibility δχ as a function of temperature after subtracting the paramagnetic contribution. The δχ starts to increase below 100±10 K, coincident with the starting temperature of the two-fold symmetry of in-plane resistivity. **(e)** The susceptibility at zero-field cooling shows a good screening signal, suggesting our LTO films are of high quality.

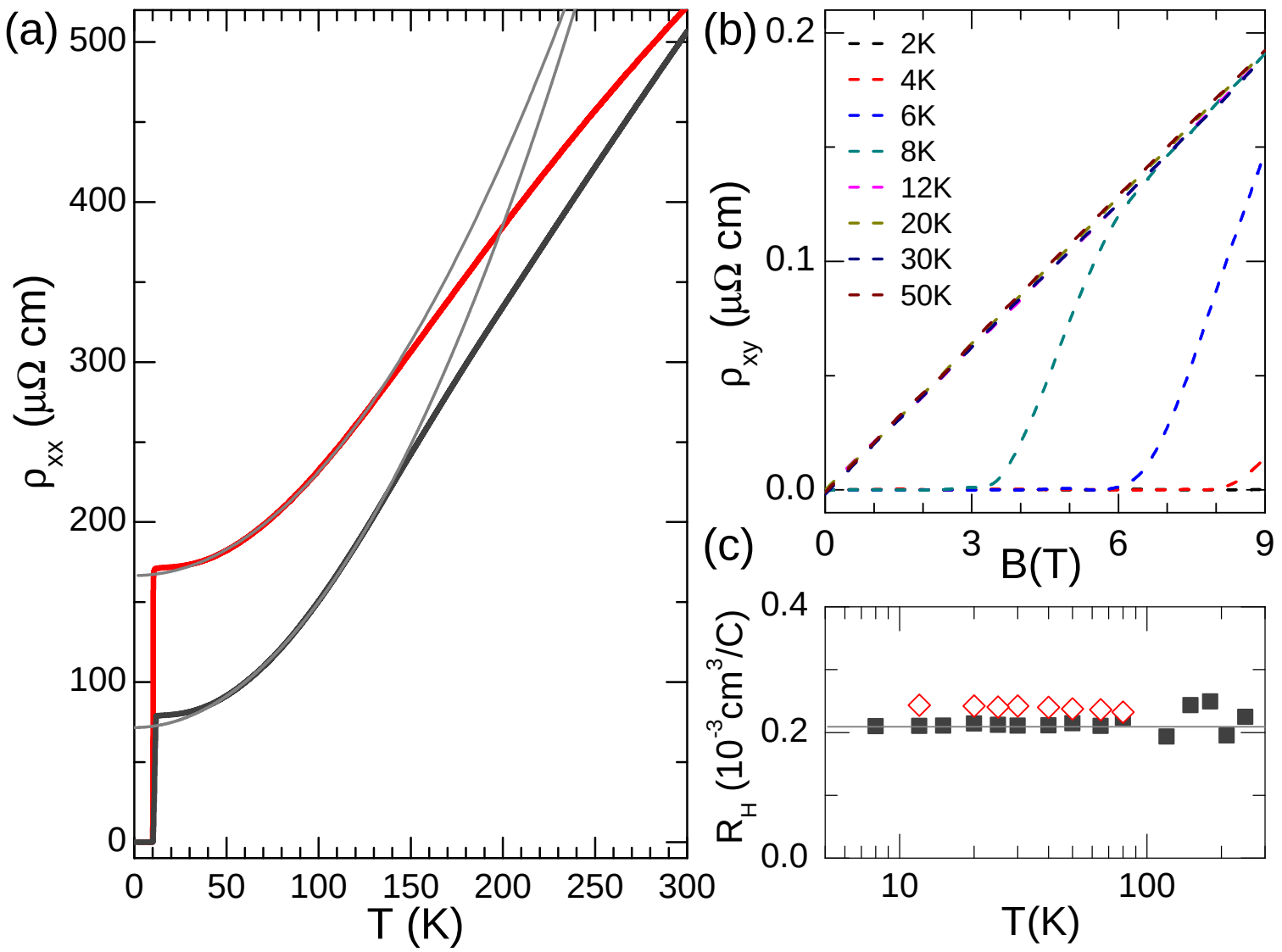
(a)
500
400
300
200
100
0
ρ_{xx} (μΩ cm)
0
50
100
150
200
250
300
T (K)
(b)
0.2
0.1
0.0
ρ_{xy} (μΩ cm)
2K
4K
6K
8K
12K
20K
30K
50K
0
3
6
9
B(T)
(c)
0.4
0.2
0.0
R_H (10^{-3}cm^3/C)
10
100
T(K)

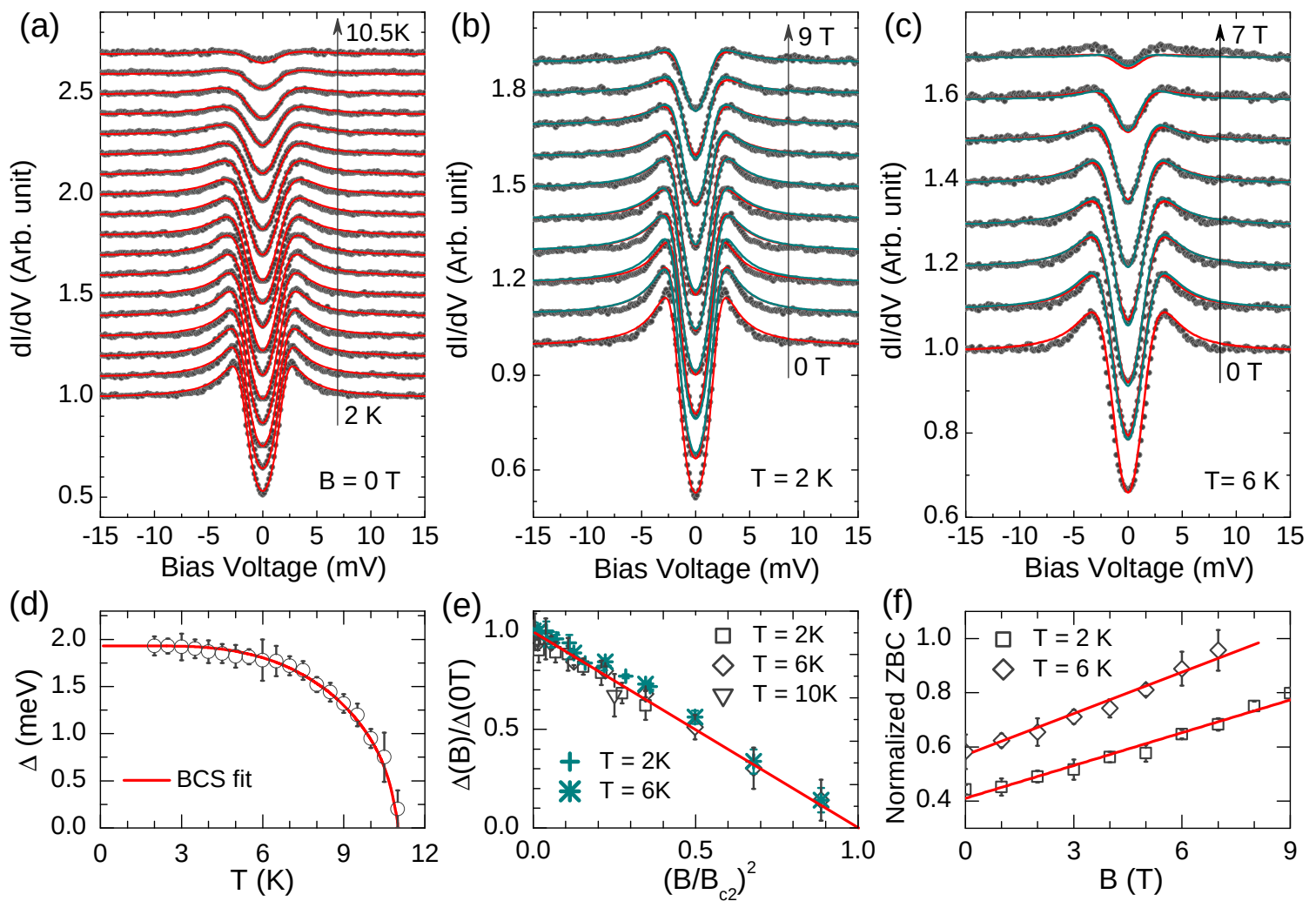
(a)
10.5K
2 K
B = 0 T
dI/dV (Arb. unit)
Bias Voltage (mV)
(b)
9 T
0 T
T = 2 K
dI/dV (Arb. unit)
Bias Voltage (mV)
(c)
7 T
0 T
T= 6 K
dI/dV (Arb. unit)
Bias Voltage (mV)
(d)
BCS fit
Δ (meV)
T (K)
(e)
T = 2K
T = 6K
T = 10K
T = 2K
T = 6K
Δ(B)/Δ(0T)
(B/B$_{c2}$)^2
(f)
T = 2 K
T = 6 K
Normalized ZBC
B (T)

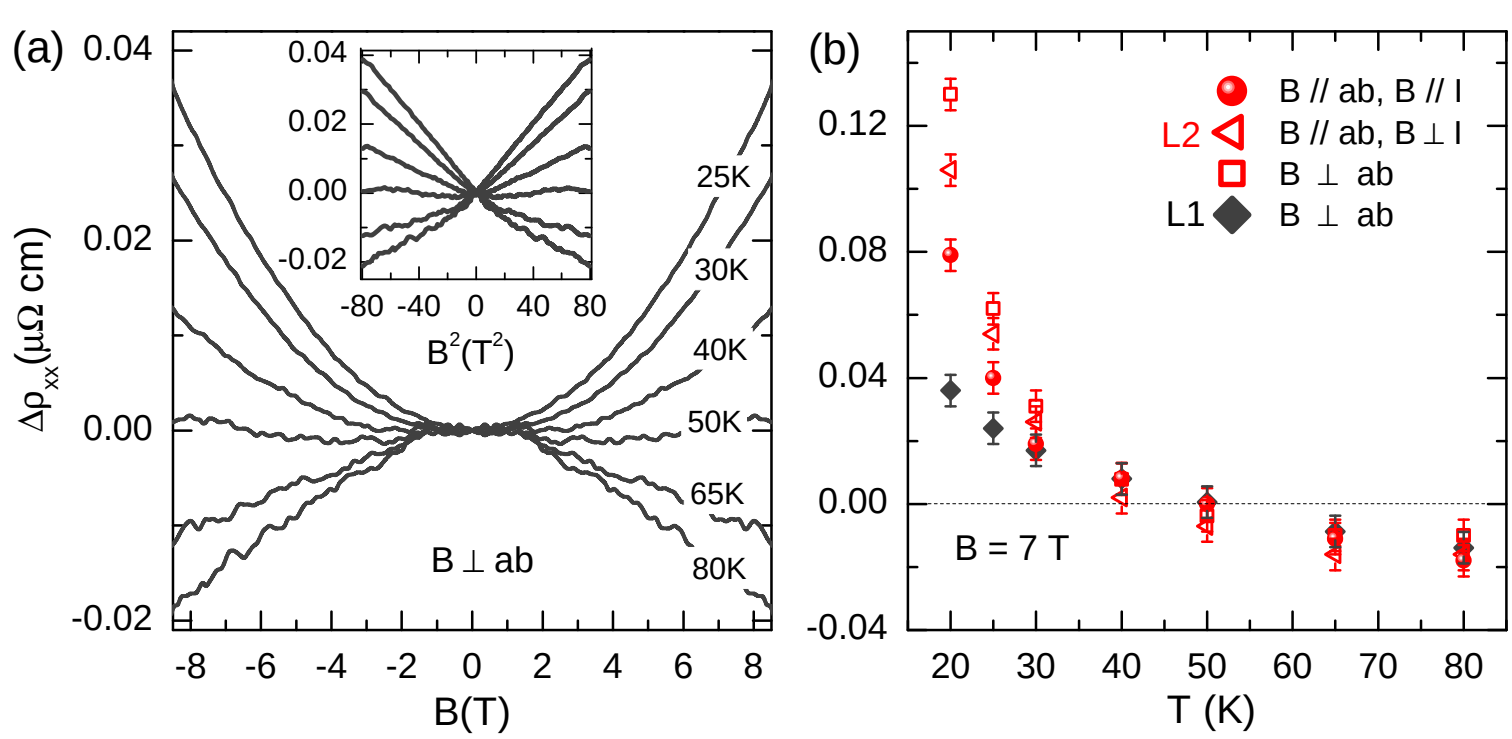
(a)
0.04
0.02
0.00
-0.02
$\Delta\rho_{xx}$(μΩ cm)
-8 -6 -4 -2 0 2 4 6 8
B(T)
25K
30K
40K
50K
65K
80K
B ⊥ ab
0.04
0.02
0.00
-0.02
-80 -40 0 40 80
$B^2(T^2)$
(b)
0.12
0.08
0.04
0.00
-0.04
20 30 40 50 60 70 80
T (K)
B // ab, B // I
L2
B // ab, B ⊥ I
B ⊥ ab
L1
B ⊥ ab
B = 7 T

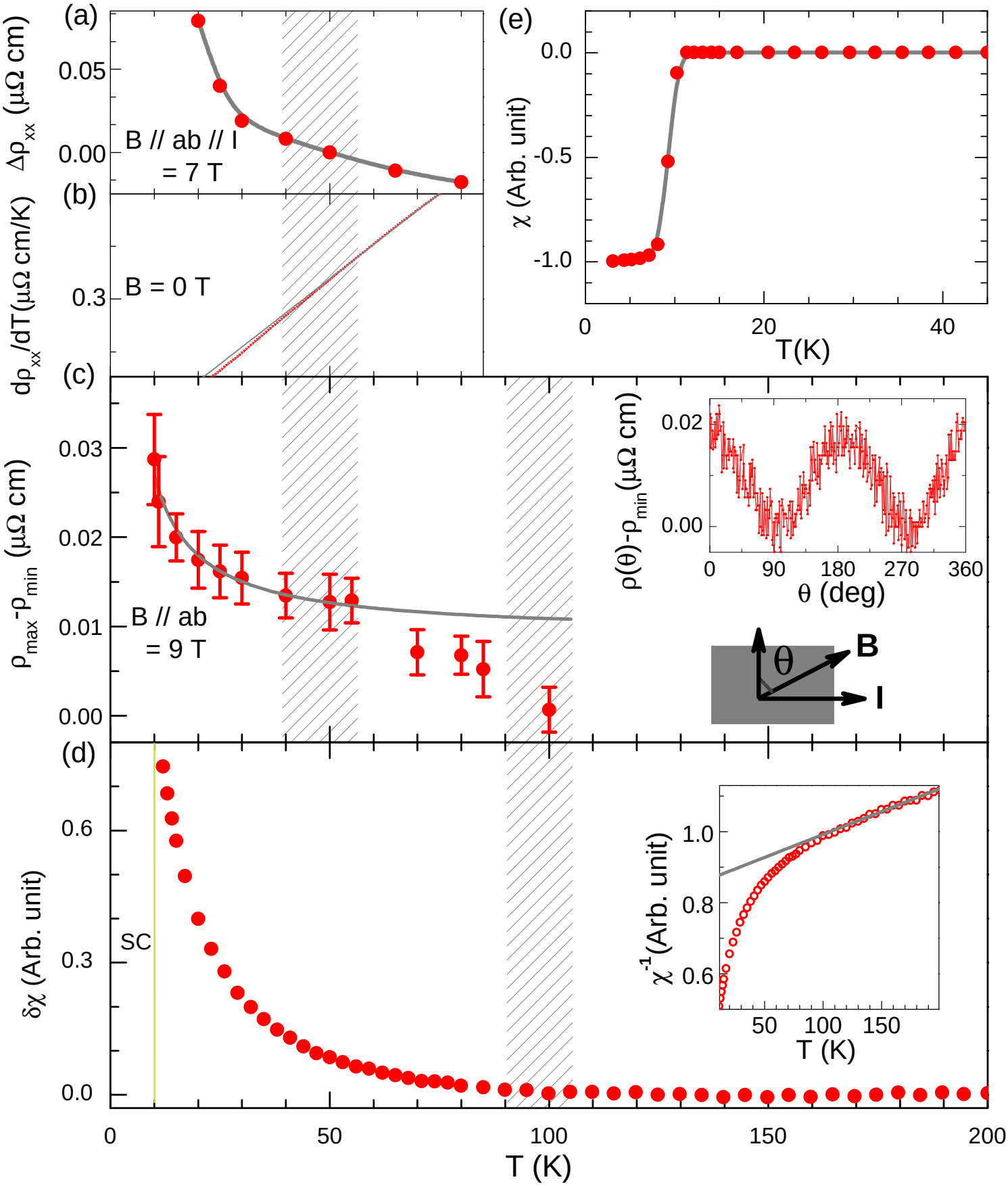
(a)
0.05
0.00
B // ab // I
= 7 T
$\Delta\rho_{xx}$ (μΩ cm)
(b)
B = 0 T
0.3
$d\rho_{xx}/dT$(μΩ cm/K)
(e)
0.0
-0.5
-1.0
χ (Arb. unit)
0
20
40
T(K)
(c)
0.03
0.02
0.01
0.00
ρ_{max}-ρ_{min} (μΩ cm)
B // ab
= 9 T
$\rho(\theta)$-ρ_{min}(μΩ cm)
0.02
0.00
0
90
180
270
360
θ (deg)
θ
B
I
(d)
0.6
0.3
0.0
δχ (Arb. unit)
SC
χ^{-1}(Arb. unit)
1.0
0.8
0.6
50
100
150
T (K)
0
50
100
150
200
T (K)

Supplementary Information

K. Jin[1,2,3], G. He[1], X. Zhang[3,4], S. Maruyama[4], S. Yasui[4], R. Suchoski[4], J. Shin[4], Y. Jiang[3], H.S. Yu[1], J. Yuan[1], L. Shan[1,2], F.V. Kusmartsev[5], R. L. Greene[3], I. Takeuchi[4]

[1]Beijing National Laboratory for Condensed Matter Physics, Institute of Physics, Chinese Academy of Sciences, Beijing 100190, China

[2]Collaborative Innovation Center of Quantum Matter, Beijing, 100190, China

[3]Center for Nanophysics and Advanced Materials and Department of Physics, University of Maryland, College Park, Maryland 20742, USA

[4]Department of Materials Science and Engineering, University of Maryland, College Park, Maryland 20742, USA

[5]Department of Physics, Loughborough University, Loughborough LE11 3TU, United Kingdom

Supplementary Figures

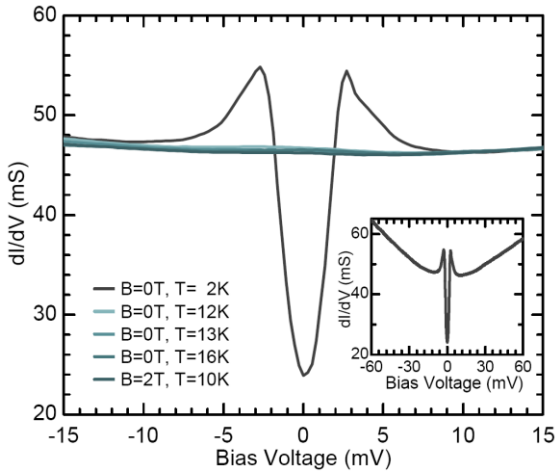

Figure S1 Point-contact spectra of a Pt-Ir tip/LTO film junction. The main panel shows differential conductance at 2, 12, 13, 16 K (0 T), and 10 K (2 T) to demonstrate the normalization procedure. The inset shows the raw spectrum data at 2 K in zero field.

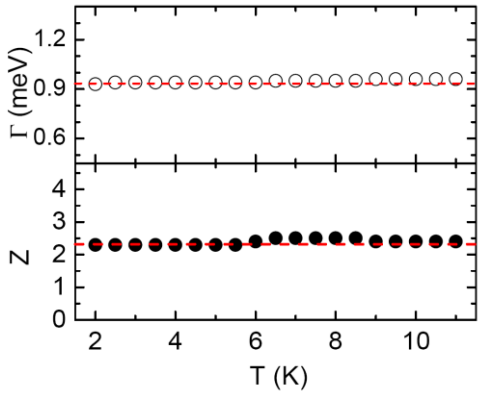

Figure S2 Temperature dependence of fitting parameters, Γ and Z, in zero field.

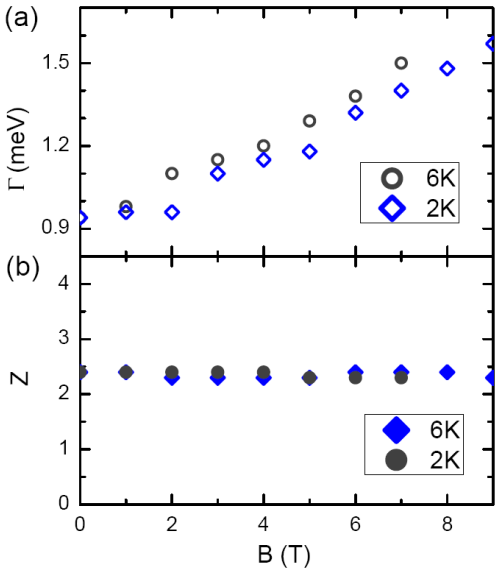

Figure S3 Field dependence of fitting parameters, Γ and Z, at 2K and 6 K. Z is constant but Γ increases with increasing field, extracted from the red fitting curves in Figure 2b and 2c. Here, the enhancement of Γ is due to the pair-breaking effect by field.

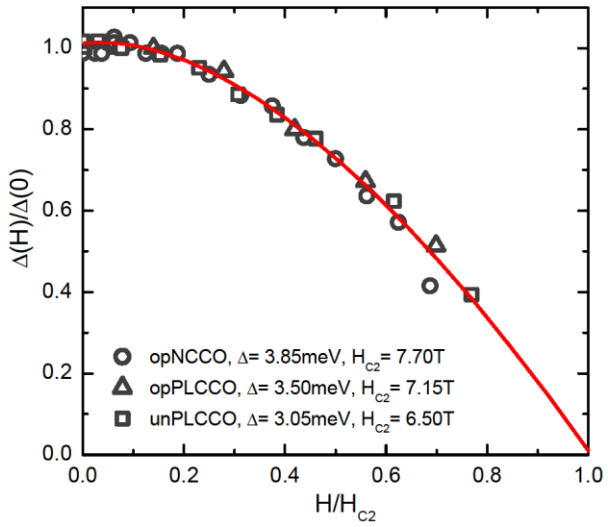

Figure S4 Magnetic field dependence of superconducting energy gap of optimal-doped (op) of NCCO, PLCCO and under-doped (un) PLCCO systems. The experimental data (symbols) obey $\Delta(H)/\Delta(0) = 1 - (H/H_{c2})^2$ (red line).

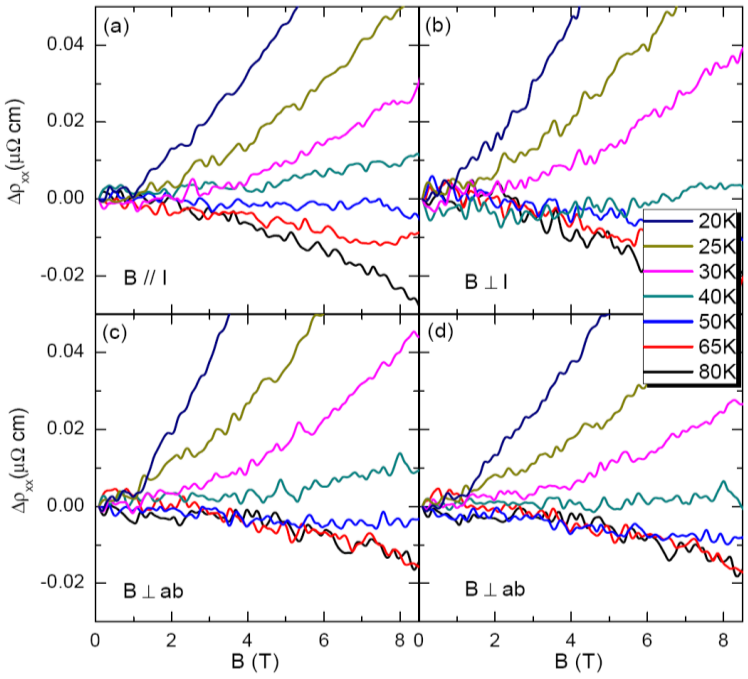

Figure S5 Magnetoresistivity versus temperature with different field directions on sample L2. The magnetic field was applied along three different directions, i.e., in the *ab*-plane with *B* // *I* (a), *B* ⊥ *I* (b) and *B* ⊥ *ab* plane (c) (d). (c) (d) show data taken from different parts of the same sample L2.

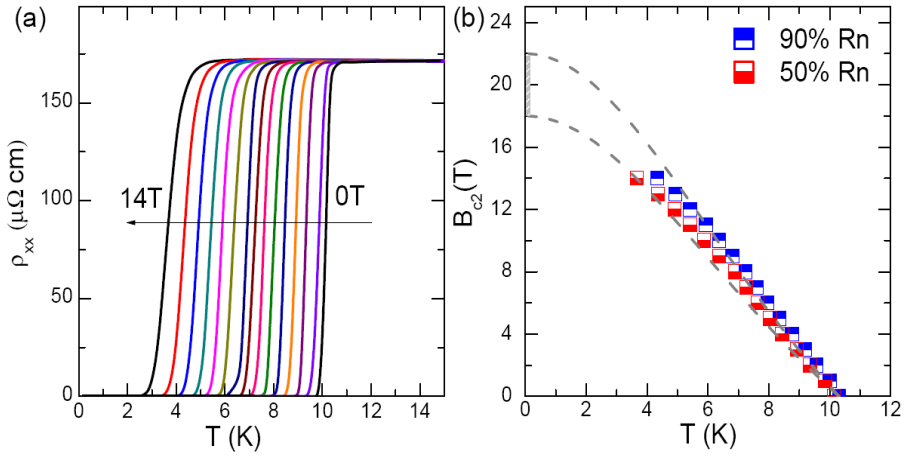

Figure S6 Resistivity and upper critical field of the sample L2. (a) ρ(T) in fields (B$\perp$*ab* plane) shows that even 14 Tesla cannot suppress the superconductivity. (b) Upper critical fields defined as the values of 90% and 50% of normal state resistivity (Rn) plotted against the temperature. The experimental data can be fitted by $B_{c2}(T) = B_{c2}(0)[1-(\mathrm{T}/\mathrm{T_c})^2\,]/[1+(\mathrm{T}/\mathrm{T_c})^2]$ derived from the Ginzburg-Landau theory.

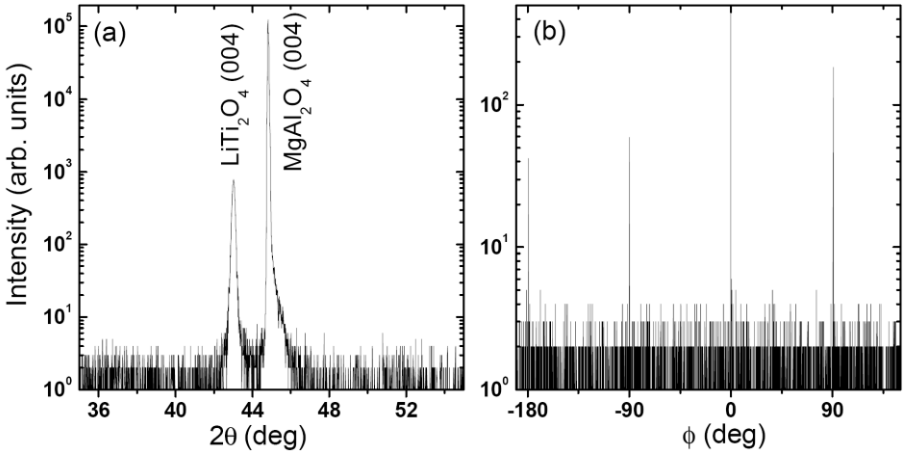

Figure S7 X-ray diffraction of LTO thin films. (a) The θ-2θ scan indicates *c*-axis oriented growth. (b) The φ-scan of the (404) reflection.

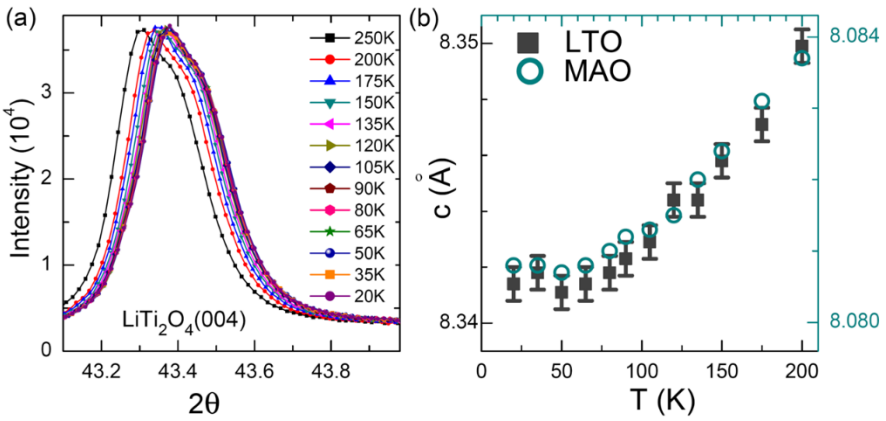

Figure S8 Temperature dependence of X-ray diffraction data and lattice parameters. (a) LTO (004) peak at different temperatures. (b) Temperature dependent *c*-axis parameter values for both the LTO film and the $MgAl_2O_4$ (MAO) substrate were extracted from X-ray diffraction measurements. They both shrink gradually as temperature decreases. The rate of change with temperature (thermal expansion) is roughly consistent with previous reports on bulk materials (S13, S14).

1) Method to normalize the tunneling spectra

In point-contact spectroscopy measurements, the actual measured voltage is comprised of the signal from the junction (dV/dI) in series with a sample resistance (R_s). In the superconducting (SC) state R_s equals zero, while in the non-SC state, the contribution from R_s has to be removed before carrying out the normalization. At low temperatures, the upper critical field of $LiTi_2O_4$ (LTO) is beyond the applied magnetic field in this experiment, so we choose the normal state spectra either at $T > T_c$ or at $B > B_{c2}$ as the reference to normalize the spectra below T_c. From the main text, it can be seen that the resistivity of LTO is almost flat at low T. This is why the spectra overlap with each other at 10 K (2 T), 12, 13, 16 K (0 T), and thus can be used as references to normalize the spectra below T_c (see Figure S1). The normalized data were obtained via

$$(dV/dI)_{normalized} = \frac{(dV/dI)_S}{(dV/dI)_N - R_S} \quad (1)$$

where $(dV/dI)_s$ represents data below T_c, and $(dV/dI)_N$ refers to the data at 10 K (2 T), 12, 13, 16 K (0 T). Meanwhile, $V = V_m - IR_s$, with V_m the applied bias voltage and V the actual bias on the junction. According to the BTK theory, the normalized dV/dI should be equal to 1 at high bias, namely

$$\left(\frac{dV}{dI}\right)_S \Big/ \left[\left(\frac{dV}{dI}\right)_N - R_S\right] = 1 \quad (2)$$

Then we can get the sample resistance R_S and also the normalized conductance (Figure 2 in the main text). The raw data of differential conductance at 2 K and 0 T are shown in the inset of Figure S1 as a function of the bias voltage up to 60 mV. An asymmetrical background appears at higher bias which also has been observed previously in other superconducting systems (S1). We symmetrized the raw spectrum by averaging the signal in negative and positive bias. Note that the asymmetry at lower bias is small, and the uncertainty in determining the fitting parameters is straightforward and contained in the error bars in all the related Figures.

2) Fitting parameters

We use the BTK theory to fit the tunneling spectra data, which contain three parameters (Δ, Z, Γ). The Z and Γ are constant for changing temperature in zero field as seen in Figure S2. In fields, two methods were used to fit the spectra, i.e., the two-channel model (S2) and the modified BTK model with an enhanced Γ in field (S3).

When a two-channel model derived from the BTK model was used to fit the spectra, a roughly constant Γ was used because the pair-breaking effect by field was separated and expressed as a normal channel superposed onto the superconducting channel. However, if the effect due to field was taken as a part of contribution to Γ, then we found the Γ increased with increasing the field (see Figure S3). In general, pair-breaking processes result in a smearing of the DOS at the gap edges, similar to the DOS in the modified BTK theory described by E' = E + iΓ. Regardless of the method used, we always arrive at the simple relation $\Delta \sim B^2$.

3) Zero bias conductance

The normalized zero bias conductance (ZBC) is given by

$$\frac{\sigma}{\sigma_N}(V=0) = (1+Z^2)\int dE[1+A(E)-B(E)]\left(-\frac{\partial f(E+eV)}{\partial V}\right)\Bigg|_{V=0} \qquad (3)$$

where f(E), A(E), and B(E) represent the Fermi distribution, probability of Andreev reflection, and the probability of ordinary reflection, respectively. Note that the intrinsic ZBC should be obtained as $Z \rightarrow \infty$. Going to a larger Z will reduce the normalized ZBC very little as $Z > 1.5$

(S4). In our calculations, the reduction by larger Z was negligible since $Z = 2.4$ in our case, as seen in Figure 2f in the main text.

The normalized ZBC at 2 K and 6 K shows a linear dependence on the magnetic field (see Fig. 3f), indicating a linear increase of the vortex density with uncorrelated vortices. Such relation has been reported in systems such as overdoped $Bi_2Sr_2CaCu_2O_{8+\delta}$ (Bi2212 intercalating with $HgBr_2$ molecules) (S5), nanosized Pb islands on a silicon wafer (S6). The departure from the linearity between ZBC and field was observed in MgB_2 (S7) and YNi_2B_2C (S8), which are multiband superconductors. In the $Ca_{2-x}Na_xCuO_2Cl_2$ (x = 0.14), the field dependence goes as $B\log B$, which is suggested to be an indication of dirty *d*-wave superconductor (S9).

4) Quadratic relation between Δ and B

To the best of our knowledge, the quadratic field dependence of the superconducting gap is formally reported for the first time in the present work. As discussed in the main text, the Maki formula will not generate a simple relation $\Delta \sim B^2$ instead, $|\Delta|^2 \sim -B$ would be expected if the pair-breaking factor is a small value compared to k_BT. However, if there exists an additional anisotropic axis due to symmetry breaking, for example, due to orbital ordering or background nematicity, $\Delta \sim -B^2$ could result as discussed in the following.

To simplify the discussion without loss of generality, we assume that the superconducting order parameter is a 3-component vector, $\mathbf{\Delta} = (\Delta_x, \Delta_y, \Delta_z)$. Then the isotropic gap is equal to the modulus of this vector: $\Delta_0 = \mathbf{(\Delta\cdot\Delta)^{1/2}} = (\Delta_x^2 + \Delta_y^2 + \Delta_z^2)^{1/2}$. In zero field, the orientation of the local spin of the Cooper pair changes in real space, while the value of the gap does not change. Therefore, the average magnetic moment of Cooper pairs vanishes, that is $\langle\mathbf{\Delta(r)}\rangle = \mathbf{0}$. However, in magnetic field, **B**, the magnetic moments of Cooper pairs can be partially polarized and therefore the susceptibility, χ, can develop a paramagnetic component, so that $\chi_{super} = \chi_{para} + \chi_{dia}$. Here, the last term is the conventional diamagnetic susceptibility of a superconductor.

To estimate the first term χ_{para}, we use the methods of invariants and note that for a cubically symmetric crystal, all thermodynamic and response functions should depend on the symmetry invariance of the cubic group O_h, which are in lowest quadratic approximation corresponding to the spherical group $O(3)$. As such, the susceptibility χ_{para} should be a function of the magnetic moments of the Cooper pairs which contribute to the symmetry invariants. There are in general three symmetry invariants here. The first one is just $\mathbf{\Delta\cdot\Delta}$, the second one is $\mathbf{\Delta\cdot B}$. The additional anisotropy axis, e.g. orbital ordering or background nematicity associated with some vector **b** results in another invariant as $\mathbf{\Delta\cdot b}$. In the vicinity of the phase transition, we can use the Taylor expansion to obtain:

$$\chi_{para}((\mathbf{\Delta\cdot b}), (\mathbf{\Delta\cdot B})) = \chi_{para}(0, 0) + \chi'_{para}(0, 0)\,(\mathbf{\Delta\cdot b}) + \chi'_{para}(0, 0)\,(\mathbf{\Delta\cdot B}) + (\text{high order terms}) \quad (4)$$

Here we assume that $(\mathbf{\Delta\cdot b})$ is positive, and in general, we take its modulus.
In using this expression, the total free energy of the superconductor in the lowest order with superconducting order parameter can be written in the form:

$$F(\mathbf{\Delta}) = \alpha\,(\mathbf{\Delta\cdot\Delta}) + \beta\,(\mathbf{\Delta\cdot\Delta})^2 + \mathbf{M\cdot B} \quad (5)$$

where the magnetization of the superconductor is equal to $\mathbf{M}= \chi_{super}\mathbf{B}$. After the substitution of the expressions for the appropriate susceptibilities, we obtain the final expression for the free energy

$$F(\mathbf{\Delta}) = \alpha\,(\mathbf{\Delta}\cdot\mathbf{\Delta}) + 2\delta\,(\mathbf{\Delta}\cdot\mathbf{b})\,(\mathbf{B}\cdot\mathbf{B}) + \mu\,(\mathbf{B}\cdot\mathbf{B}) + (\text{ high order terms}) \quad (6)$$

Minimization of this expression with respect to the vector order parameter, $\mathbf{\Delta}$, after some algebraic manipulations, gives the following equation for the superconducting energy gap $\Delta = (\mathbf{\Delta}\cdot\mathbf{\Delta})^{1/2}$:

$$\alpha\,\Delta + 2\,\beta\,\Delta^3 = \pm\delta\,b\,B^2 \quad (7)$$

here b is the modulus of the vector **b.** Introducing the notation for the gap in the zero magnetic field as $\Delta(B=0)= \Delta(0)= \Delta_0 = (-\alpha/2\beta)^{1/2}$ we can finally obtain

$$\Delta(B)= \Delta_0 - \delta\,b\,B^2/2\,|\alpha| \quad (8)$$

Here α, β, δ are the parameters of the Ginzburg-Landau expansion. Thus, the gap value has a quadratic dependence on magnetic field. Note that as usual $\alpha=a(T-T_c)$ and β, δ are temperature independent constants. The superconductivity in the proposed orbital ordered state is expected to have a vector order parameter, describing an effective spin of Cooper pairs. This vector order parameter is associated with the three-fold degeneracy of the t_{2g} bands of 3*d* electrons. The specific form of the order parameter depends on the details of the pairing mechanism. However in general, in systems with degenerate bands, nontrivial spin pairing may arise which is associated with an isotropic s-type gap.

We also checked the tunneling spectra of junctions with $(Nd, Ce)_2CuO_4$ (NCCO) and $(Pr, La, Ce)_2CuO_4$ (PLCCO) systems and discovered that they also exhibit the $\Delta \sim -B^2$ relation, as shown in Figure S4. Naturally, cuprates and LTO are very different from each other in many ways, and yet, they both exhibit the same behavior. This indicates that perhaps occurrence of symmetry breaking leading to the vector order parameter is a rather common phenomenon, and this can be used to probe signs of symmetry breaking induced by orbital (and other types of) ordering.

5) Magnetoresistivity and the upper critical field

Magnetoresistivity (MR) in LTO changes from positive to negative as temperature is increased. The negative MR is nearly isotropic, whereas the positive MR shows clear anisotropy (see Figure 3b and S5). The observed MR is positive above superconducting transition temperature in the proposed orbital ordered (OO) nematic state, and negative above the orbital ordering transition. In the (OO) nematic phase, the coherence of the Landau quasi-particles is significantly improved, and the Fermi-liquid approach may be applicable as in normal metals. But in ordinary metals, the application of a magnetic field parallel to the thin film does not usually lead to any dramatic changes in the transport properties. However, for a 2D electron gas in the strongly

correlated Fermi liquid regime, the positive magnetoresistance comes about due to electron-electron interactions (S10, S11) and has the following form:

$$\Delta R(B,T) \propto \left(\frac{B}{T}\right)^2 \tag{9}$$

In both cases, when it is perpendicular to the applied current *I* and when it is parallel to the applied current *I,* the magnetic field has small effect on the orbital motion of the electrons (unless the field is very strong).

When the OO nematic state is destroyed at $T > 40$ K, there may still be some "fluctuating" islands. We call them "fluctuating" because they may be not stable and have some finite life time, but they serve as additional (magnetic) scattering centers for the electron transport. When the magnetic field is applied, some of these islands dissolve away and the resistivity decreases. Indeed, this is similar to the negative magnetoresistance phenomena observed by Bergman when he covered thin metallic Mg films with small controlled quantities of a magnetic ion like Fe, or a heavy ion with large spin-orbit coupling like Au (S12). With the increase of the density of the spin-orbit scattering centers, he observed dramatic changes in the size and sign of magnetoresistance as a function of field: the magnetoresistance changed from negative to positive with increasing number of spin-orbit scattering centers. This is very similar to what we observe in LTO.

From the temperature dependence of resistivity in fields, we extracted the upper critical field. As shown in Fig. S6, the B_{c2} at 90% and 50% of normal state resistivity (Rn) can be fitted by $B_{c2}(T) = B_{c2}(0)[1-(\mathrm{T}/\mathrm{T_c})^2\,]/[1+(\mathrm{T}/\mathrm{T_c})^2]$ derived from the Ginzburg-Landau theory. Extrapolating to the zero temperature limit, we get B_{c2} to be between 18 and 22 Tesla.

6) Structure characterizations

The $LiTi_2O_4$ has a cubic symmetry (*Fd3m*). The lithium cations, Li^+ are located at the tetrahedral 8*a* sites. The titanium cations, Ti^{3+} and Ti^{4+} are occupying the octahedral 16*d* sites. Our LTO thin films grown on (00*l*)-$MgAl_2O_4$ (MAO) substrates show pure (00l) peaks, indicaitng *c*-axis orientation. The φ-scan using the (404) reflection confirms that LTO films are epitaxailly grown (Fig. S7). Temperature dependence of an X-ray diffraction peak reveals a smooth thermal expansion as shown in Fig. S8.

References

S1. Shan L. *et al*. Distinction between the normal-state gap and superconducting gap of electron-doped cuprates. *Phys. Rev. B* **78**, 014505 (2008).

S2. Smith, C. W. & Dolan, P. J. Determining transport parameters for superconductor/normal metal point contacts at fixed temperature from conductance versus magnetic field data. *Physica C* **471**, 285-289 (2011).

S3. Daghero, D. & Gonnelli, R. S. Probing multiband superconductivity by point-contact spectroscopy. *Supercond. Sci. & Tech*. **23**, 043001 (2010).

S4. Blonder, G. E., Tinkham, M. & Klapwijk. T. M. Transition from metallic to tunneling regimes in superconducting microconstrictions: Excess current, charge imbalance, and supercurrent conversion. *Phys. Rev. B* **25**, 4515-4532 (1982).

S5. Krasnov, V. M., Kovalev, A. E., Yurgens, A. & Winkler, D. Magnetic field dependence of the superconducting gap and the pseudogap in Bi2212 and $HgBr_2$-Bi2212, studied by intrinsic tunneling spectroscopy. *Phys. Rev. Lett.* **86**, 2657-2660 (2001).

S6. Ning, Y. X. *et al*. Observation of surface superconductivity and direct vortex imaging of a Pb thin island with a scanning tunneling microscope. *Europhys. Lett.* **85,** 27004 (2009).

S7. Eskildsen, M. R. *et al*. Scanning tunneling spectroscopy on single crystal MgB_2. *Physica C* **385,** 169 (2003).

S8. Mukhopadhyay, S., Sheet, G., Raychaudhuri, P., & Takeya, H. Magnetic-field dependence of superconducting energy gaps in YNi_2B_2C: Evidence of multiband superconductivity. *Phys. Rev. B* **72**, 014545 (2005).

S9. Hanaguri, T. *et al*. Coherence factors in a high-T_c cuprate probed by quasi-particle scattering off vortices. *Science* **323**, 923-926 (2009).

S10. Lee, P. A. & Ramakrishnan, T. V. Magnetoresistance of weakly disordered electrons, *Phys. Rev. B* **26**, 4009-4012 (1982).

S11. Lee, P. A. & Ramakrishnan, T. V. Disordered electronic systems, *Rev. Mod. Phys.* **57,** 287-337 (1985).

S12. Bergman, G. Measurement of the magnetic scattering time by weak localization. *Phys. Rev. Lett.* **49**, 162-164 (1982).

S13. Johnston, D. C., Swenson, C. A. & Kondo, S. Specific heat (1.2–108 K) and thermal expansion (4.4–297 K) measurements of the 3*d* heavy-fermion compound LiV_2O_4. *Phys. Rev. B* **59**, 2627-2641 (1999).

S14. Geng, H. X. *et al.* Investigations on preparation, upper critical field and low temperature thermal expansion of $LiTi_2O_4$ superconductor. *Physica C* **432**, 53-58 (2005).